List-Mode Maximum Likelihood Reconstruction of Compton Scatter Camera Images in Nuclear Medicine[1]

Scott J. Wilderman, N.H. Clinthorne, J.A. Fessler, and W. Les Rogers
University of Michigan

Abstract

A Maximum Likelihood (ML) image reconstruction technique using list-mode data has been applied to Compton scattering camera imaging. List-mode methods are appealing in Compton camera image reconstruction because the total number of data elements in the list (the number of detected photons) is significantly smaller than the number of possible combinations of position and energy measurements, leading to a much smaller problem than that faced by traditional iterative reconstruction techniques. For a realistic size device, the number of possible detector bins can be as large as 10 billion per pixel of the image, 3 or 4 orders of magnitude more than the number of counted photons. One difficulty in applying the list-mode technique is in determining the parameters which describe the response of the imaging system. In this work, a simple method for determining the required system matrix coefficients is employed, in which a back-projection is performed in list-mode, and response coefficients determined for only tallied pixels. Projection data has been generated for a representative Compton camera system by Monte Carlo simulation for disk sources with hot and cold spots at various energies and list-mode maximum likelihood reconstructions performed on the simulated data.

I. INTRODUCTION

Reconstruction of images from Compton aperture projection data is a computationally challenging task. To date, no exact, analytical solutions applicable to a practical imaging device have been found. Nor have traditional iterative reconstruction techniques (such as Maximum Likelihood (ML) Expectation Maximization (EM)) proven tractable, primarily because of the enormous size of the matrix required to describe a viable imaging system. For the C-SPRINT system [1] consisting of a 81 cm square scatter detector (with 1.2 mm spatial resolution and with energy recorded in 100 eV bins), and a cylindrical capture detector 25 cm in radius and 10 cm long (spatial resolution of 3 mm), the number of elements of the system matrix M_S is roughly 2.3×10^{10} per pixel of the image. For an NxN $2D$ image, direct reconstruction would involve inversion of $M_S N^2$ dimensional matrices, and iterative methods would require $\sim 10^{14}$ recursive multiplications [2].

Since, in the general case, the number of detected events N_γ will be much smaller than the number of system elements M_S in the full projection data set, list-mode reconstruction methods present themselves as possible alternatives to other solution algorithms [3, 4, 5]. In such methods, each detected event is treated as a point in a continuous measurement space, rather than as contributing a count to a position and energy bin. Since $N_\gamma << M_S$, the sizes of the matrices are greatly reduced and so the number of operations required in solving the problem are reduced by a like amount. In addition, this technique has the advantage of preserving accuracy of measurement data that might otherwise be lost in discretizing of energy and position during the binning procedure.

The conventional(*i. e.* , using binned data) ML problem for the Compton camera can be posed as follows: Let Y be the measured projection data, accumulated in bins as the number of counts for a given combination of scatter detector element, capture detector element, and scattering energy bin (with the number of counts in each bin denoted Y_i), and $\underline{\lambda}$ the underlying pixelated object, each pixel having an intensity given by λ_j. Then (ignoring random coincidences)

$$Y \sim \text{Poisson}\left\{T\underline{\lambda}\right\}, \tag{1}$$

and the log-likelihood has the form

$$\log f(Y|\underline{\lambda}) = \sum_i Y_i \log \sum_j t_{ij}\lambda_j - \sum_i \sum_j t_{ij}\lambda_j . \tag{2}$$

In solving for $\underline{\lambda}$ using the iterative EM algorithm, the maximization step can be written as

$$\left. \frac{1}{\lambda_j} \sum_i Y_{ij}^E - s_j \right|_{\lambda_j = \lambda_j^{(l+1)}} = 0 \tag{3}$$

and the expectation step as

$$Y_{ij}^E = Y_i \frac{\lambda_j t_{ij}}{\sum_k t_{ik}\lambda_k} \tag{4}$$

leading to the iteration (indexed by l)

$$\lambda_j^{(l+1)} = \frac{\lambda_j^{(l)}}{s_j} \sum_i \frac{Y_i t_{ij}}{\sum_k t_{ik}\lambda_k^{(l)}}. \tag{5}$$

In the above, s_j is the probability that a photon emitted from pixel j would be detected anywhere, and t_{ij} the probability that a γ emitted from pixel j is collected in bin i, so

$$s_j = \sum_i t_{ij}.$$

In the list mode case, we approximate Y by considering that each event is measured in a unique bin, so that $Y_i \to 1$ for each detected particle, and $Y_i \to 0$ for the infinite number of

[1]This work has been partially supported through Contract NCI 2RAO1 CA-32846-24.

possible events not detected in the current measurement. The sums over the M_S system bins become instead sums over just the N_γ detected events. Barrett *et al.* [4] and Parra [5] have proven that this approximation on Y holds (here we ignore any time dependence of the measurement), with the one exception that as the detected Y_i no longer span the space of all possible events, $s_j \neq \sum_i t_{ij}$, but rather, s_j is now the integral over all possible events i, including those for which $Y_i = 0$.

In this paper we develop analytical expressions for t_{ij} and s_j in the list-mode case for a Compton scatter camera, and estimate them using rather severe approximation. We then present images reconstructed from Monte Carlo simulations for disk sources with hot and cold spots at a variety of energies.

II. METHODS

In a Compton scatter camera, the sequence of physical events which leads to a count being registered begins with the emission of a photon at $\mathbf{z}_0$ in direction Ω_1, followed by Compton scattering at position $\mathbf{z}_1$ through an angle Ω_c (with energy loss E_c) and final absorption at $\mathbf{z}_2$. The coefficients t_{ij} are then the probabilities that a photon emitted from j will be measured as event i described by the quantities $\mathbf{z}_1, E_c$, and $\mathbf{z}_2$ (henceforth the vector of data describing event i is denoted $\mathbf{A}_i$, after Parra [5]). As the spatial and energy resolution of the detection system is finite, the measurements are imprecise and t_{ij} will be be given by the integral over the pixel volume of the density function $p(\mathbf{A}'|\mathbf{z}_0)$ describing the probabilities of an emission from j producing a 'real' event $\mathbf{A}'$, convolved with a function $p(\mathbf{A}_i|\mathbf{A}')$ describing the measurement process, or

$$t_{ij} = \int_{\mathbf{z}_0 \in V_j} d\mathbf{z}_0 p(\mathbf{z}_0) \int d\mathbf{A}' p(\mathbf{A}_i|\mathbf{A}') p(\mathbf{A}'|\mathbf{z}_0). \quad (6)$$

Here $\mathbf{z}_0 \in V_j$ indicates that the integral is taken over only those $\mathbf{z}_0$ in the pixel volume V_j, and $p(\mathbf{z}_0)d\mathbf{z}_0$ is the probability that a particle was emitted in $d\mathbf{z}_0$ at $\mathbf{z}_0$. Note that

$$p(\mathbf{A}_i|\mathbf{A}') = p(\mathbf{z}_1|\mathbf{z}_1')p(\mathbf{z}_2|\mathbf{z}_2')p(E_c|E_c'),$$

and so the integral over $\mathbf{A}'$ implies an integral over all possible real collision positions and energy transfers which could have resulted in the measurement $\mathbf{A}_i$. We also have

$$s_j = \int_{\mathbf{z}_0 \in V_j} d\mathbf{z}_0 p(\mathbf{z}_0) \int d\mathbf{A}' p(\mathbf{A}'|\mathbf{z}_0). \quad (7)$$

where now the integral over $\mathbf{A}'$ is the integral over all possible real collisions, independent of the measurements. If we assume a mono-energetic source and that absorption in the second detector is complete (or that incomplete absorptions are eliminated by energy discrimination), we can determine an expression for $p(\mathbf{A}'|\mathbf{z}_0)$ by breaking the physical process in a sequence of events and determining the probability of each process. In the determination of the probabilities it will be easier to represent $\mathbf{z}_1$ in terms of a direction Ω_1 and distance r_1 determined by $\mathbf{z}_1 - \mathbf{z}_0$. Note then that $d\mathbf{z}_1 = r_1^2 d\Omega_1 dr_1$. We will similarly think of $\mathbf{z}_2$ in terms of Ω_c (the Compton scattering angle) and r_2, determined by $\mathbf{z}_2 - \mathbf{z}_1$. Using these variables, the events are their probabilities can be described as (we omit the primes on all the variables, but recognize that we are referring to real events and not measurements):

1. $p(\Omega_1|\mathbf{z}_0)d\Omega_1$, that the photon was emitted at $\mathbf{z}_0$ in initial direction Ω_1 in $d\Omega_1$ toward $\mathbf{z}_1$
2. P_{esc}^{obj}, that it then escaped the object
3. $p(r_1, \Omega_c)dr_1 d\Omega_c$, that it then Compton scattered in dr_1 at r_1 and emerged with direction Ω_c in $d\Omega_c$ toward $\mathbf{z}_2$
4. $p(E_c|\Omega_c)dE_c$, that it lost energy E_c in dE_c during the scattering collision (this factor accounts for the Doppler broadening of the emitted photon spectrum)
5. P_{esc}^{det1}, that the scattered photon escaped the detector
6. $p_{abs}^{det2}(r_2)dr_2$, that it was then absorbed in the second detector in dr_2 at r_2

In the above, all the probabilities are actually conditioned on all the previous events in the sequence having occurred. Analytic expressions for the probabilities described above are given by:

$$\begin{aligned} p(\Omega_1|\mathbf{z}_0) &= \frac{1}{4\pi r_1^2} \\ P_{esc}^{obj} &= \int dt_1 e^{-\mu_{tot}^{obj}(t_1)t_1} \\ p(r_1, \Omega_c) &= \left[\int dt_1 e^{-\mu_{tot}^{det1}(t_1)t_1}\right] \mu^{det1}(\Omega_c, r_1)/r_2^2 \\ p(E_c|\Omega_c) &= D_{op}(E_c|\Omega_c) \\ P_{esc}^{det1} &= \int dt_2 e^{-\mu_{tot}^{det1}(E_\gamma, t_2)t_2} \\ p_{abs}^{det2}(r_2) &= \left[\int dt_2 e^{-\mu_{tot}^{det2}(E_\gamma, t_2)t_2}\right] \mu_{abs}^{det2}(E_\gamma, r_2) \end{aligned} \quad (8)$$

In the equations above, the function t describes the track length inside a medium (it will have a different functional form in each medium) along the corresponding direction, and the $\mu(t)$'s the total, Compton, and absorption linear attenuation coefficients in the various media, as denoted by the superscripts and subscripts. D_{op} refers to the shape of the Doppler broadening, and E_γ is the initial energy minus E_c.

Computation of t_{ij} and s_j by this approach, which involves stepping through each object pixel j and determining the integrals of equations 6 and 7, requires detailed knowledge of the detector system, and even knowledge of the initial source distribution of object, $p(\mathbf{z}_0)$. We begin by making the rather severe approximation that there is no Doppler broadening, so $D_{op}(E_c|\Omega_c) = \delta(E_c - \alpha_c(\Omega_c))$, where $\alpha_c(\Omega_c)$ is the energy transfer in the collision, determined strictly by momentum conservation. We next assume that the measurements are perfect, implying $p(\mathbf{A}_i|\mathbf{A}') = \delta(\mathbf{A}' - \mathbf{A}_i)$, and that the attenuation coefficients are constant in the detectors. We get then

$$t_{ij} = p(\mathbf{A}_i) \int_{\mathbf{z}_0 \in V_j} d\mathbf{z}_0 \times p(\mathbf{z}_0) \delta(\mathbf{z}_0 - \mathbf{z}_0(\Omega_c, \mathbf{z}_1, \mathbf{z}_2)) \quad (9)$$

$$\left[\int dt_1 e^{-\mu_{tot}^{obj}(t_1)t_1^{obj}}\right]\mu_{tot}^{det1}e^{-\mu_{tot}^{det1}t_1^{det1}}.$$

In the above, $\delta(\mathbf{z}_0-\mathbf{z}_0(\Omega_c,\mathbf{z}_1,\mathbf{z}_2))$ refers to only those $\mathbf{z}_0$ which are possible given that Ω_c is fixed by conservation of momentum and that Ω_1 is fixed by $(\mathbf{z}_1-\mathbf{z}_0)$ and $(\mathbf{z}_2-\mathbf{z}_1)$. The function $p(\mathbf{A}_i)$ is given by the remaining component probabilities of t_{ij} evaluated at $\mathbf{A}_i$:

$$\begin{aligned} p(\mathbf{A}_i) = \quad & \frac{1}{4\pi}\mu_c(\Omega_c)e^{-\mu_{tot}^{det1}(\alpha_\gamma)t_2^{det1}} \\ & \times \mu_{abs}^{det2}(\alpha_\gamma)e^{-\mu_{tot}^{det2}(\alpha_\gamma)t_2^{det2}} \end{aligned} \tag{10}$$

We note that the result of (10 is equivalent to that developed by Parra [5] after application of Bayes's rule to (6). The integrand of equation 10 corresponds to $p(\mathbf{A}_i)p(\mathbf{z}_0|\mathbf{A}_i)$, in Parra, where $p(\mathbf{z}_0|\mathbf{A}_i)$ is the probability of an emission having taken in area $d(\mathbf{z}_0)$ at $\mathbf{z}_0$ for a given $\mathbf{A}_i$. The factor $p(\mathbf{A}_i)$ of (10) is equivalent to Parra's $p(\mathbf{A}_i)$, with appropriate normalization by other factors which are independent of the object pixel. We observe that we could have reached (10) by applying Bayes' rule to (6) to yield

$$t_{ij} = \int_{\mathbf{z}_0\in V_j} d\mathbf{z}_0 \int d\mathbf{A}' p(\mathbf{A}_i)p(\mathbf{z}_0|\mathbf{A}')p(\mathbf{A}'|\mathbf{A}_i) \tag{11}$$

and then using our same approximations. Note that the expression (7) for s_j is not greatly simplified at this point, as only the integral over the Doppler broadening function is resolved under the current approximations.

We now proceed by noting the δ function describing the possible $\mathbf{z}_0$ in the integral of (10) traces out a cone B_c in the image space which is uniquely determined by each $\mathbf{A}_i$, so our integral over $\mathbf{z}_0 \in V_j$ is actually an area integral over the surface of B_c within j. We now assume that $p(\mathbf{z}_0)$ is uniform over the pixel volume, and note that in equation 4, t_{ij} appears in both the numerator and denominator and that as the sum in the denominator is over only the pixels j, $p(\mathbf{A}_i)$ can be ignored in (10), as can all other constants in the integrand. We arrive at:

$$t_{ij} \propto \int_{B_c(\mathbf{z}_0\in V_j)} d\mathbf{z}_0 \left[\int dt_1 e^{-\mu_{tot}^{obj}(t_1)t_1^{obj}}\right] e^{-\mu_{tot}^{det1}t(\mathbf{z}_0,\mathbf{z}_1)}. \tag{12}$$

We now restrict ourselves to the $2D$ case (note that this provides only slight relief from the complexity of the original equation 6 for t_{ij}, as only P_{esc}^{obj} and $p(\mathbf{z}_0)$ are dependent on the object), so that $e^{-\mu_{tot}^{obj}t_1} = 1$, and the surface integrals for t_{ij} become line integrals in the image plane, with $d\mathbf{z}_0 = dl/||\mathbf{z}_1 - \mathbf{z}_0||$. We ignore the thickness of the first detector and assume that $r_1 = ||\mathbf{z}_1 - \mathbf{z}_0||$ is constant across the area of pixel j so that the t_{ij} are now given by just the path length of B_c inside j divided by r_1 (with $\mathbf{z}_0$ taken to be the center of the pixel). The original expression (7) for s_j is still not much changed, requiring integrals over all Ω_1, r_1, Ω_c and r_2, in addition to the integral over $\mathbf{z}_0$. So we now argue that in $2D$, s_j can be taken to be constant with little impact on the estimates of λ. This assumption is reasonable because in $2D$ we eliminate attenuation in the object, the primary determinant in non-uniformity in s_j. Clinthorne has shown that errors in estimates of λ are a function of the degree of non-uniformity of the s_j [7], and as in $2D$ variations in s_j will be limited primarily to differences in subtended solid angles, for small objects at moderate distances from the detectors, the s_j's should vary slowly and the impact of the constant s_j approximation should be fairly small. Note that under the current approximations, neither t_{ij} nor s_j are dependent on the configuration of the detector, but instead are functions only of the measurements $\mathbf{A}_i$ and the orientation of the image space.

III. Results

Projection data was generated by Monte Carlo simulation using the program SKEPTIC [8]. SKEPTIC has been employed and tested extensively in numerous medical imaging applications [9], [10], including simulation of Compton scatter cameras [1], [11]. The program writes to disk lists of the exact interaction positions and energy losses, and the uncertainties in the measurements of these quantities are simulated by sampling from appropriate Gaussian distributions describing the energy and spatial resolution of the component detectors, as described in [6]. Doppler broadening of the scattered gamma spectrum, which has recently been found to be a limiting factor in the resolution performance of Compton cameras [12], is modeled using the tabulated data of Biggs [13] for atomic silicon and of Reed [14] for crystalline silicon. The list-mode reconstruction program reads this data and applies the back-projection algorithm of [11] to determine the coefficients t_{ij}, which are stored. The iterative procedure is then simple matrix multiplication. The detector system modeled is the C-SPRINT silicon and NaI system proposed by Clinthorne and LeBlanc [1]. The scatter detector consists of a 9x9 cm array of Si elements, divided into 1.2 mm cells. Each cell is 5 mm thick and assumed to have an energy resolution of roughly 250 eV, (an achievable level, as suggested by Weilhammer [15]). The capture detector is taken to be a hollow cylinder of NaI, 25 cm in radius and 10 cm long, with a spatial resolution of 3 mm. ^{99m}Tc, and ^{131}I and annihilation photon sources were modeled. The test configuration was a 5 cm radius disk (with uniform background intensity 1) containing 2 hot spots (intensity 2) and 2 cold spots (intensity 0) with 1.0 and .5 cm radii, at a distance of 10 cm from the face of the scatter detector. Emissions were sampled from a continuous position distribution on the disk until 200,000 Compton events were collected. Reconstructions were performed on a 32 by 32 grid of 5 mm pixels. For the current work, the number of particles is contrained by the storage requirements for the t_{ij}.

Initial computation of the t_{ij}'s consumed roughly 10 minutes of CPU on a Ultra Sparc 1 workstation (with 128 MB RAM), and iterations over λ took 30 seconds each. An initial image (corresponding to an unfiltered back-projection) was determined by $\lambda_j^{(0)} = \sum_i t_{ij}$. Results are shown below for all three test energies in figures 1 - 6. For each of the 3 energies, a first figure shows the image after the initial back-projection, and the second after 65 or 75 iterations. The quality of the images is degraded primarily by noise (the realtivelly small number of counts) and the effects of Doppler broadening on the approximations for t_{ij} and s_j. It is also noted that the geometry of the C-SPRINT detector tends to maximize the penalty due to the Doppler effect (which is most severe at the technetium energy). Nevertheless, in all 3 cases, both hot and both cold spots are in evidence.

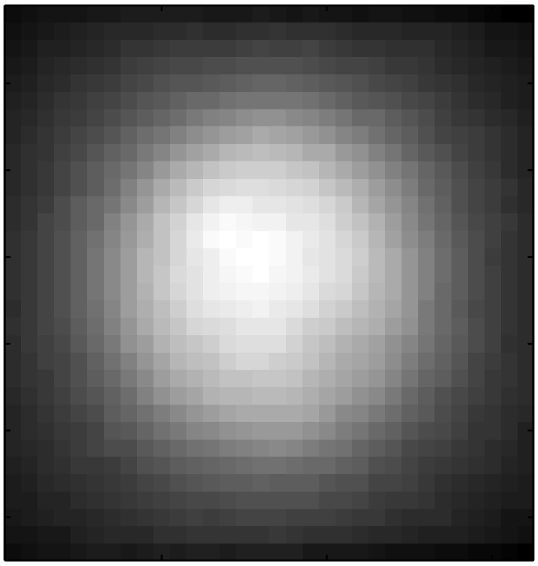

Figure 1: 141 keV Initial back-projected image

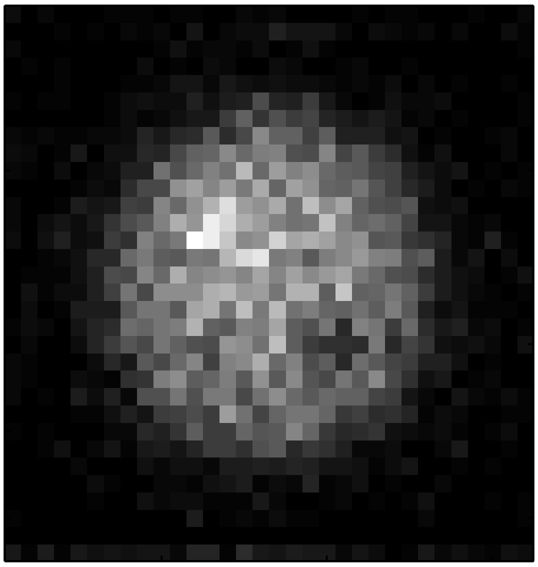

Figure 2: 141 keV Image after 75th iteration

Because of the relatively few number of counts, a roughness penalty was introduced. Equation 3 is recast as

$$\frac{1}{\lambda_j}\sum_i Y_{ij}^E - s_j - \alpha \sum_k r_{jk}\lambda_k = 0. \tag{13}$$

Here the coefficients r_{jk} are 0 except for the 4 nearest and 4 next nearest pixels k relative to j, and set so that $\sum_j \sum_k r_{jk} = 0$. The expectation step of equation 4 remains the same, but now

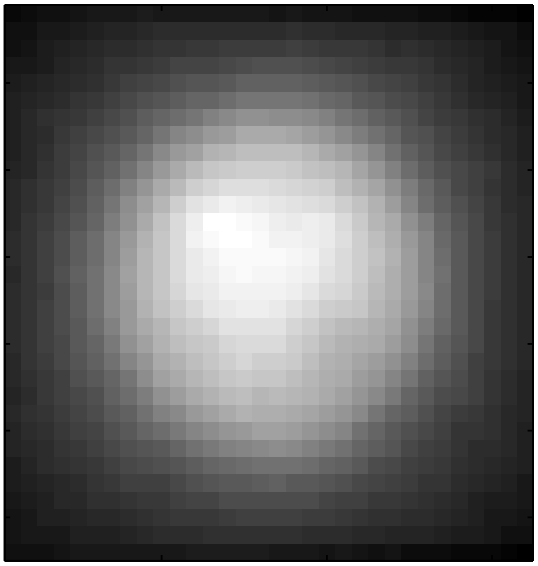

Figure 3: 364 keV Initial back-projected image

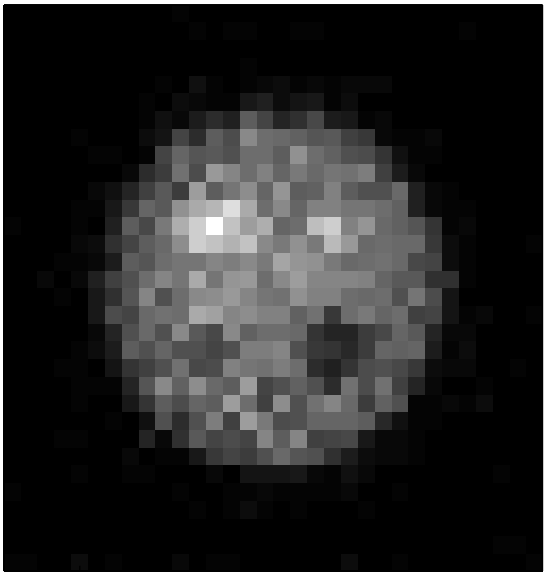

Figure 4: 364 keV Image after 75th iteration

the maximization step requires solving for a quadratic equation in λ_j (which roughly doubled the CPU usage per iteration). For the current work, α is set to some fraction α_0 times the constant s_j divided by $\overline{\lambda^{(0)}}$, the average value of $\lambda^{(0)}$ taken from the back-projection. Some reconstructions are presented in figures 7 through 10 for α_0 ranging from 0.005 to 0.01. Image quality is greatly enhanced at all three energies.

IV. Conclusions

Expressions for the coeffients t_{ij} and s_j required for list-mode maximum likelihood reconstruction of Compton scatter cameras have been developed. A penalized EM algorithm has been applied to simulated projection data in

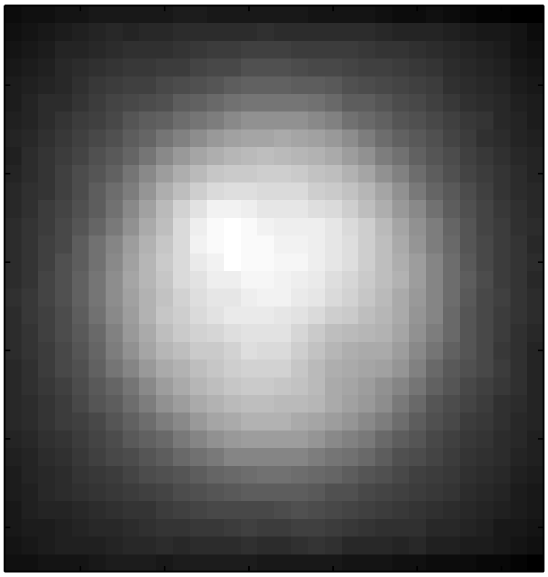

Figure 5: 511 keV Initial back-projected image

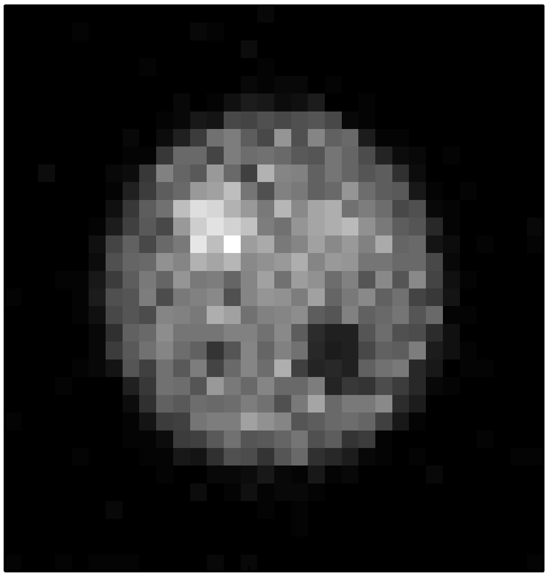

Figure 6: 511 keV Image after 65th iteration

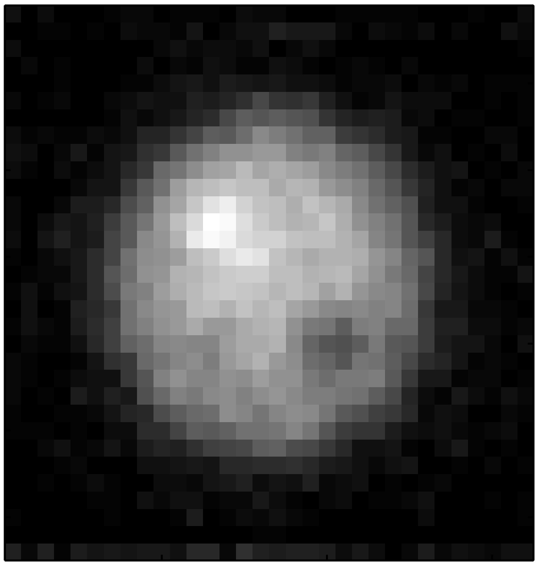

Figure 7: Regularized ($\alpha_0 = 0.005$) 141 keV Image after 75th iteration

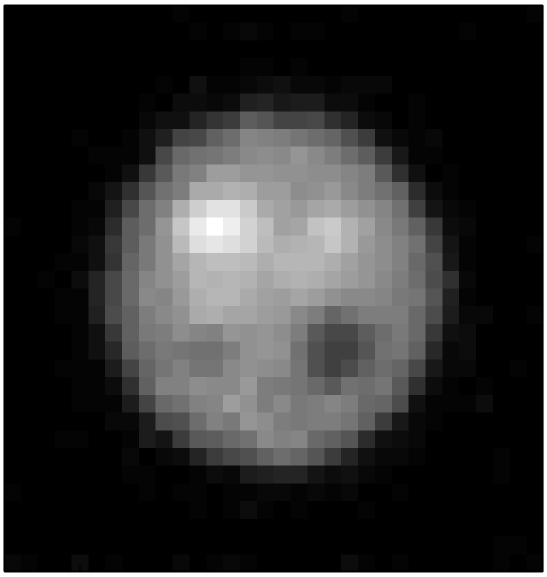

Figure 8: Regularized ($\alpha_0 = 0.005$) 364 keV Image after 50th iteration

$2D$ with very good results over a range of energies, using a crude approximation of the imaging system and a relatively small number of counts. Improvements can be expected by employing more realistic approximations of the Doppler and measurement convolution functions, and then developing approximations for the probablities in equations 9 which permit analytic or numerical evaluation of the integrals of (7) and (6) or (11). Future work should include parallelization of the algorithm to permit larger number of particles, and approximations applicable in $3D$.

V. REFERENCES

[1] J.W. LeBlanc, N.H. Clinthorne, C-h. Hua, E. Nygard, W.L. Rogers, D.K. Wehe, P. Weilhammer, S.J. Wilderman, "C-Sprint: A prototype Compton camera system for low energy gamma ray imaging", presented at *IEEE Nucl. Sci. Sym. and Med. Imaging Conf., Albuquerque, N.M., 1997.*

[2] L. Shepp and Y. Vardi, "Maximum likelihood reconstruction for emission tomography," *IEEE Trans. Med. Imag., vol. MI-1, 1984* pp. 113-122.

[3] T. Hebert, R. Leahy, M. Singh, "Three-dimensional maximum-likelihood reconstruction for an electronically collimated single-photon-emission imaging system," *J. Opt. Soc. Am., vol. 7, 1990* pp. 1305-1313.

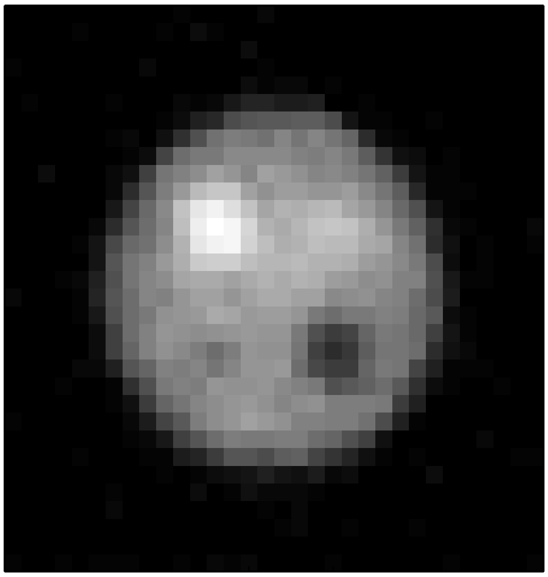

Figure 9: Regularized ($\alpha_0 = 0.005$) 511 keV Image after 75th iteration

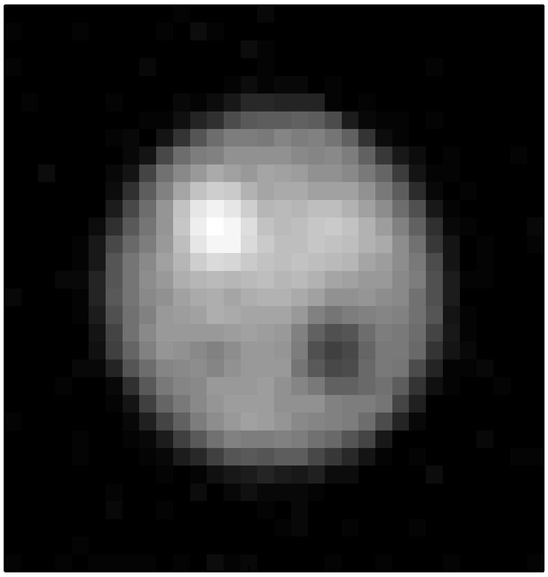

Figure 10: Regularized ($\alpha_0 = 0.010$) 511 keV Image after 100th iteration

[4] H.H. Barrett, T. White, and L.C. Parra, “List-mode likelihood,” *J. Opt. Soc. Am., vol. 14, 1997* pp. 2914-2923.

[5] L.C. Parra and H.H. Barrett, “List-mode likelihood: EM algorithm and image quality estimation demonstrated on 2-D PET,” *IEEE Trans. Med. Imag., vol. 17, 1998* pp. 228-235.

[6] S.J. Wilderman, W.L. Rogers, G.F. Knoll and J.C. Engdahl, ”Fast Algorithm for List-Mode Back-Projection of Compton Scatter Camera Data,” IEEE Trans. Nucl. Sci., *in press.*

[7] N.H. Clinthorne, “Noise Propegation from Attenuation Measurements into PET Emission Reconstructions,” presented at *IEEE Nucl. Sci. Sym. and Med. Imaging Conf, Toronto, Ontario, 1998.*

[8] S.J. Wilderman, “Vectorized algorithms for the Monte Carlo simulation of kilovolt electron and photon transport,” *University of Michigan, Ann Arbor, MI, Ph. D. dissertation, 1990.*

[9] M.J. Flynn, S.M. Hames, S.J. Wilderman, and J.J. Ciarelli, “Quantum noise in digital x-ray image detectors with optically coupled scintillators,” *IEEE Trans. Nucl. Sci., vol. 43, 1996* pp. 2320-2325.

[10] M.C. Wrobel, N.H. Clinthorne, J.A. Fessler, Y. Zhang, S.J. Wilderman, and W.L. Rogers, “Proposed method for correcting aperture penetration in high energy slit aperture and pinhole SPECT,” *IEEE Trans. Nucl. Sci., vol. 44, 1997* pp. 1564-1570.

[11] S.J. Wilderman, W.L. Rogers, G.F. Knoll and J.C. Engdahl, “Monte Carlo calculation of point spread functions of Compton scatter cameras,” *IEEE Trans. Nucl. Sci., vol. 44, 1997* pp. 250-254.

[12] C. Ordonez, A. Bolozdynya, and W. Chang, “Energy uncertainties in Compton scatter Cameras,” presented at *IEEE Nucl. Sci. Sym. and Med. Imaging Conf, Albuquerque, N.M., 1997.*

[13] F. Biggs, L.B. Mendelsohn, and J.B. Mann, “Hartree-Fock Compton profiles for the elements,” *At. Data Nuc. Data Tables, vol. 16, 1975* pp. 201-309.

[14] W.A, Reed and P. Eisenberger, “Gamma-ray Compton profiles of diamond, silicon, and germanium,” *Phys. Rev. B, vol. 6, 1972* pp. 4598-4604.

[15] P. Weilhammer, *private communication, Nov 1996.*